Journal of Computational Physics 227 (2008) 9898–9912

Contents lists available at ScienceDirect

Journal of Computational Physics

journal homepage: www.elsevier.com/locate/jcp

Novel electromagnetic surface integral equations for highly accurate computations of dielectric bodies with arbitrarily low contrasts

Özgür Ergül, Levent Gürel *

Department of Electrical and Electronics Engineering, Bilkent University, TR-06800, Ankara, Turkey
Computational Electromagnetics Research Center (BiLCEM), Bilkent University, TR-06800, Ankara, Turkey

ARTICLE INFO

Article history:
Received 30 November 2007
Received in revised form 4 May 2008
Accepted 5 August 2008
Available online 15 August 2008

Keywords:
Dielectrics
Low contrast
Surface integral equations
Multilevel fast multipole algorithm

ABSTRACT

We present a novel stabilization procedure for accurate surface formulations of electromagnetic scattering problems involving three-dimensional dielectric objects with arbitrarily low contrasts. Conventional surface integral equations provide inaccurate results for the scattered fields when the contrast of the object is low, i.e., when the electromagnetic material parameters of the scatterer and the host medium are close to each other. We propose a stabilization procedure involving the extraction of nonradiating currents and rearrangement of the right-hand side of the equations using fictitious incident fields. Then, only the radiating currents are solved to calculate the scattered fields accurately. This technique can easily be applied to the existing implementations of conventional formulations, it requires negligible extra computational cost, and it is also appropriate for the solution of large problems with the multilevel fast multipole algorithm. We show that the stabilization leads to robust formulations that are valid even for the solutions of extremely low-contrast objects.

1. Introduction

In various physical applications, electromagnetic surface integral equations (SIEs) are commonly used to formulate problems involving dielectric objects with arbitrary shapes [1]. Using equivalent surface currents and applying the boundary conditions on the surface of the scatterer, a set of integral equations can be derived. In the literature, various SIE formulations are reported for the numerical solution of scattering problems involving three-dimensional dielectric objects [2–8]. However, those formulations become inaccurate to calculate the scattered fields as the contrast of the object decreases, i.e., when the electromagnetic material properties of the object and the host medium become close to each other. There are various applications involving scattering from low-contrast objects. Examples are narrow-band dielectric photonic crystals [9], polymeric materials [10], plastic mines buried in soil [11], and biological tissues [12], such as red blood cells in blood plasma [7,13,14]. On the other hand, it is usually difficult to investigate low-contrast structures with the SIEs, since these formulations encounter stability problems when the contrast is low and the scattered fields are weak. This breakdown, which limits the applicability of the surface formulations, does not arise in volume integral equations (VIEs). Therefore, VIEs can be used to solve such problems accurately. However, it is also desirable to extend the applicability of SIEs to low-contrast problems in order to use the advantages of the surface formulations, which may require lower numbers of unknowns compared to VIEs for some problems.

The inaccuracy of SIEs for the solution of low-contrast problems is due to insufficient modelling of the radiating parts of the equivalent currents defined on the objects [15]. By extracting the nonradiating parts of the currents and solving the modified

* Corresponding author. Address: Department of Electrical and Electronics Engineering, Bilkent University, TR-06800, Ankara, Turkey. Tel.: +90 312 290 5750; fax: +90 312 290 5755.
E-mail address: lgurel@bilkent.edu.tr (L. Gürel).

0021-9991/$ - see front matter © 2008 Elsevier Inc. All rights reserved.
doi:10.1016/j.jcp.2008.08.004

equations only for the radiating currents (similar to the volume formulations), scattered fields from low-contrast objects can be calculated accurately. Recently, we have applied this procedure to various integral-equation formulations for the solution of three-dimensional problems with arbitrary geometries [16–18]. For both the tangential (T) and normal (N) formulations, our stabilization technique involves the expansion of the incident fields in a series of basis functions and the rearrangement of the right-hand sides (RHSs) of the equations. By eliminating the terms related to the identity operators, accuracy of the formulations can be improved further at the cost of increased processing time. This stabilization procedure is simple and easily applied to the existing implementations of the conventional formulations. On the other hand, the resulting formulations are stable only for moderately low-contrast problems and they break down as the contrast is further decreased to very low values. In addition, these "quasi-stable" formulations are sensitive to how accurately the matrix elements are computed and the stable region is more limited when finite-precision methods, such as the fast multipole method (FMM) and the multilevel fast multipole algorithm (MLFMA) [3], are used in order to accelerate the solutions.

As a remedy, in this paper, we introduce a novel stabilization procedure for accurate solutions of scattering problems involving arbitrarily low-contrast dielectric objects. Similar to previous techniques, this stabilization procedure is also based on extracting the nonradiating parts of the currents. However, the RHSs of the equations are rearranged in a different manner using fictitious incident fields. Since the left-hand sides (LHSs) of the equations do not change and the modification of the RHSs requires only a few matrix–vector multiplications (MVMs) involving the operators that are already available, this stabilization procedure is also easy to implement and the extra computational cost is negligible. The technique is applied on a T formulation although it can be generalized to other existing formulations, including the N formulations. We present the results of scattering problems involving dielectric spheres of various sizes since the analytical solutions are available for these problems. We also demonstrate the improved accuracy provided by the stabilization technique on scattering problems involving a cube geometry by performing convergence analysis and comparing the results obtained by using SIEs with the results of a VIE implementation. For the solution of large problems, we use FMM and MLFMA to accelerate the MVMs required by the iterative solvers. Our results show that the stabilized equation does not break down even for the solution of scattering problems involving extremely low-contrast objects, such as a sphere of relative permittivity $1 + 10^{-9}$ in free space.

The rest of the paper is organized as follows. In the next section, we summarize the conventional surface formulations. Section 3 presents the extraction of the nonradiating currents to obtain stable formulations. Then, Section 4 introduces the novel stabilization technique based on fictitious fields. Finally, Section 5 provides numerical examples, followed by our concluding remarks in Section 6.

2. Surface formulations

In the surface formulations of scattering problems involving homogenous dielectric objects, the operators are defined as

$$\mathcal{T}_l\{\boldsymbol{X}\}(\boldsymbol{r}) = \mathrm{i}k_l \int_S \mathrm{d}\boldsymbol{r}' \left[\boldsymbol{X}(\boldsymbol{r}') + \frac{1}{k_l^2}\nabla' \cdot \boldsymbol{X}(\boldsymbol{r}')\nabla\right] g_l(\boldsymbol{r},\boldsymbol{r}'), \tag{1}$$

$$\mathcal{K}_l\{\boldsymbol{X}\}(\boldsymbol{r}) = \int_{\mathrm{PV},S} \mathrm{d}\boldsymbol{r}' \boldsymbol{X}(\boldsymbol{r}') \times \nabla' g_l(\boldsymbol{r},\boldsymbol{r}'), \tag{2}$$

$$\mathcal{I}\{\boldsymbol{X}\}(\boldsymbol{r}) = \boldsymbol{X}(\boldsymbol{r}), \tag{3}$$

for the outside ($l = 1$) and inside ($l = 2$) the object. In (1) and (2), S is the surface of the object, PV indicates the principal value of the integral, k_l is the wavenumber associated with medium l, and

$$g_l(\boldsymbol{r},\boldsymbol{r}') = \frac{\exp(\mathrm{i}k_l R)}{4\pi R} \quad (R = |\boldsymbol{r} - \boldsymbol{r}'|) \tag{4}$$

is the homogenous-space Green's function. Using the operators in (1)–(3), the general procedure of the surface formulations can be summarized as follows:

(1) Apply the operators on the equivalent surface currents $\boldsymbol{J}(\boldsymbol{r})$ and $\boldsymbol{M}(\boldsymbol{r})$ to obtain the expressions for the scattered fields. Electric and magnetic currents can be defined as

$$\boldsymbol{J}(\boldsymbol{r}) = \hat{\boldsymbol{n}} \times \boldsymbol{H}(\boldsymbol{r}), \tag{5}$$

$$\boldsymbol{M}(\boldsymbol{r}) = -\hat{\boldsymbol{n}} \times \boldsymbol{E}(\boldsymbol{r}), \tag{6}$$

where $\hat{\boldsymbol{n}}$ is the outward normal vector at a point $\boldsymbol{r}$ on the surface.

(2) Enforce the boundary conditions for the tangential electric and magnetic fields on the surface of the scatterer.

(3) Combine the outer ($l = 1$) and the inner ($l = 2$) formulations appropriately to derive a set of equations to solve for $\boldsymbol{J}(\boldsymbol{r})$ and $\boldsymbol{M}(\boldsymbol{r})$.

(4) Calculate the scattered electric and magnetic fields from $\boldsymbol{J}(\boldsymbol{r})$ and $\boldsymbol{M}(\boldsymbol{r})$.

Based on the items above, various formulations can be derived by using different combinations of the boundary conditions, testing schemes, and scaling operations. Several of them are accurate, free of the internal resonance problem, and commonly used in the literature [2–8].

When the boundary conditions are tested directly by using the tangential unit vector $\hat{\boldsymbol{t}}$ at the observation point, the T formulations are derived as [6]

$$\hat{\boldsymbol{t}}\cdot\begin{bmatrix} a\mathcal{T}_1 & -a\eta_1^{-1}\mathcal{K}_1^{+} \\ c\eta_1\mathcal{K}_1^{+} & c\mathcal{T}_1 \end{bmatrix}\cdot\begin{bmatrix}\boldsymbol{J}\\ \boldsymbol{M}\end{bmatrix}(\boldsymbol{r})+\hat{\boldsymbol{t}}\cdot\begin{bmatrix} b\mathcal{T}_2 & -b\eta_2^{-1}\mathcal{K}_2^{-} \\ d\eta_2\mathcal{K}_2^{-} & d\mathcal{T}_2 \end{bmatrix}\cdot\begin{bmatrix}\boldsymbol{J}\\ \boldsymbol{M}\end{bmatrix}(\boldsymbol{r})=-\hat{\boldsymbol{t}}\cdot\begin{bmatrix} a\eta_1^{-1}\boldsymbol{E}^{\mathrm{i}}(\boldsymbol{r}) \\ c\eta_1\boldsymbol{H}^{\mathrm{i}}(\boldsymbol{r})\end{bmatrix}, \tag{7}$$

where

$$\mathcal{K}_l^{\pm}=\mathcal{K}_l\pm 0.5\hat{\boldsymbol{n}}\times\mathcal{I}, \tag{8}$$

η_l is the impedance of the medium $l=1$ and 2, while $\boldsymbol{E}^{\mathrm{i}}(\boldsymbol{r})$ and $\boldsymbol{H}^{\mathrm{i}}(\boldsymbol{r})$ are the incident electric and magnetic fields due to the external sources. In (7), the inner and outer formulations are combined using the coupling coefficients a, b, c and d. For example, the choices $\{a=\eta_1,\ b=\eta_2,\ c=1/\eta_1,\ d=1/\eta_2\}$ and $\{a=b=c=d=1\}$ lead to Poggio–Miller–Chang–Harrington–Wu–Tsai (PMCHWT) formulation [1] and the combined T formulation (CTF) [6], respectively. Both of these formulations are free of the internal-resonance problem and provide accurate results for objects with moderate contrasts. In this paper, we apply the stabilization procedures to another T formulation obtained by using $\{a=d=\eta_1,\ b=c=\eta_2\}$, which is slightly different from CTF [16]. With these coefficients, (7) becomes

$$\hat{\boldsymbol{t}}\cdot\begin{bmatrix} \eta_1\mathcal{T}_1+\eta_2\mathcal{T}_2 & -(\mathcal{K}_1+\mathcal{K}_2) \\ \eta_1\eta_2(\mathcal{K}_1+\mathcal{K}_2) & \eta_2\mathcal{T}_1+\eta_1\mathcal{T}_2 \end{bmatrix}\cdot\begin{bmatrix}\boldsymbol{J}\\ \boldsymbol{M}\end{bmatrix}(\boldsymbol{r})=-\hat{\boldsymbol{t}}\cdot\begin{bmatrix} \boldsymbol{E}^{\mathrm{i}}(\boldsymbol{r}) \\ \eta_2\eta_1\boldsymbol{H}^{\mathrm{i}}(\boldsymbol{r})\end{bmatrix}, \tag{9}$$

which is completely free of the identity operators (like the PMCHWT formulation) and involves well-balanced diagonal blocks (like CTF) when the contrast is low.

In contrast to the T formulations, N formulations involve a projection operation using the unit normal vector $\hat{\boldsymbol{n}}$. Combining the inner and outer formulations, we obtain

$$\hat{\boldsymbol{n}}\times\begin{bmatrix} a\mathcal{K}_1^{+} & a\eta_1^{-1}\mathcal{T}_1 \\ -c\eta_1\mathcal{T}_1 & c\mathcal{K}_1^{+} \end{bmatrix}\cdot\begin{bmatrix}\boldsymbol{J}\\ \boldsymbol{M}\end{bmatrix}(\boldsymbol{r})-\hat{\boldsymbol{n}}\times\begin{bmatrix} b\mathcal{K}_2^{-} & b\eta_2^{-1}\mathcal{T}_2 \\ -d\eta_2\mathcal{T}_2 & d\mathcal{K}_2^{-} \end{bmatrix}\cdot\begin{bmatrix}\boldsymbol{J}\\ \boldsymbol{M}\end{bmatrix}(\boldsymbol{r})=-\hat{\boldsymbol{n}}\times\begin{bmatrix} a\boldsymbol{H}^{\mathrm{i}}(\boldsymbol{r}) \\ -c\boldsymbol{E}^{\mathrm{i}}(\boldsymbol{r})\end{bmatrix}, \tag{10}$$

where different choices for the coupling coefficients are again available. Among these, the choices $\{a=\mu_1,\ b=\mu_2,\ c=\epsilon_1,\ d=\epsilon_2\}$ and $\{a=b=c=d=1\}$ lead to N-Müller formulation [5] and the combined N formulation (CNF) [6], respectively, which are both free of the internal-resonance problem. In this paper, we consider the conventional and stable forms of CNF. Inserting the coefficients in (10), CNF can be written as

$$-\begin{bmatrix}\mathcal{I} & 0\\ 0 & \mathcal{I}\end{bmatrix}\cdot\begin{bmatrix}\boldsymbol{J}\\ \boldsymbol{M}\end{bmatrix}(\boldsymbol{r})+\hat{\boldsymbol{n}}\times\begin{bmatrix} \mathcal{K}_1-\mathcal{K}_2 & \eta_1^{-1}\mathcal{T}_1-\eta_2^{-1}\mathcal{T}_2 \\ -\eta_1\mathcal{T}_1+\eta_2\mathcal{T}_2 & \mathcal{K}_1-\mathcal{K}_2 \end{bmatrix}\cdot\begin{bmatrix}\boldsymbol{J}\\ \boldsymbol{M}\end{bmatrix}(\boldsymbol{r})=-\hat{\boldsymbol{n}}\times\begin{bmatrix} \boldsymbol{H}^{\mathrm{i}}(\boldsymbol{r}) \\ -\boldsymbol{E}^{\mathrm{i}}(\boldsymbol{r})\end{bmatrix}. \tag{11}$$

2.1. Comments on T and N formulations

Using a Galerkin scheme and choosing the same set of basis and testing functions for the discretization, N formulations in (10) contain well-tested identity operators. These strong interactions are located on the diagonal blocks of the matrix equations. On the other hand, T formulations in (7) contain weakly-tested identity operators on the non-diagonal blocks, which may vanish as in (9). Because the T and N formulations have different forms of identity operators, the two formulations show different behaviors in terms of conditioning and accuracy:

(1) Due to their well-tested identity operators, N formulations are usually better-conditioned than the T formulations [6,7,19]. Therefore, iterative solutions of the N formulations are easier; this is essential, especially when the problem size is large. To obtain rapid convergence with the T formulations, iterative solvers can be accelerated by employing preconditioners.

(2) Although they are better conditioned, N formulations can be considerably less accurate compared to the T formulations for the same discretization [6]. This inaccuracy is also observed in the solution of perfectly conducting objects with the magnetic-field integral equation, which is also an N formulation [20,21]. The source of the error is the identity operators. In this paper, we use Rao–Wilton–Glisson (RWG) [22] basis functions to expand the unknown current densities. Choosing a more appropriate set of basis functions [23–26] and applying a regularization to smooth the identity operators [27] are among the possible ways to improve the accuracy of the N formulations.

2.2. Low-contrast breakdown of conventional formulations

As the contrast goes to zero, i.e., $\epsilon_2 \to \epsilon_1$ and $\mu_2 \to \mu_1$, the T formulation in (9) becomes

$$\hat{\boldsymbol{t}} \cdot \begin{bmatrix} 2\eta_1\mathcal{T}_1 & -2\mathcal{K}_1 \\ 2\eta_1^2\mathcal{K}_1 & 2\eta_1\mathcal{T}_1 \end{bmatrix} \cdot \begin{bmatrix} \boldsymbol{J} \\ \boldsymbol{M} \end{bmatrix}(\boldsymbol{r}) = -\hat{\boldsymbol{t}} \cdot \begin{bmatrix} \boldsymbol{E}^{\mathrm{i}}(\boldsymbol{r}) \\ \eta_1^2\boldsymbol{H}^{\mathrm{i}}(\boldsymbol{r}) \end{bmatrix}. \tag{12}$$

In addition, the incident fields due to the external sources satisfy the set of identities [18]

$$\begin{Bmatrix} \hat{\boldsymbol{t}}\cdot \\ \hat{\boldsymbol{n}}\times \end{Bmatrix} \begin{bmatrix} \eta_1\mathcal{T}_1 & -\mathcal{K}_1 \\ \mathcal{K}_1 & \eta_1^{-1}\mathcal{T}_1 \end{bmatrix} \cdot \begin{bmatrix} \hat{\boldsymbol{n}} \times \boldsymbol{H}^{\mathrm{i}} \\ -\hat{\boldsymbol{n}} \times \boldsymbol{E}^{\mathrm{i}} \end{bmatrix}(\boldsymbol{r}) = -0.5 \begin{Bmatrix} \hat{\boldsymbol{t}}\cdot \\ \hat{\boldsymbol{n}}\times \end{Bmatrix} \begin{bmatrix} \boldsymbol{E}^{\mathrm{i}}(\boldsymbol{r}) \\ \boldsymbol{H}^{\mathrm{i}}(\boldsymbol{r}) \end{bmatrix}. \tag{13}$$

Consequently, the solution of (12) can be obtained as $\boldsymbol{J}(\boldsymbol{r}) = \hat{\boldsymbol{n}} \times \boldsymbol{H}^{\mathrm{i}}(\boldsymbol{r})$ and $\boldsymbol{M}(\boldsymbol{r}) = -\hat{\boldsymbol{n}} \times \boldsymbol{E}^{\mathrm{i}}(\boldsymbol{r})$. When the contrast is zero, CNF in (11) reduces to a simpler form, i.e.,

$$-\begin{bmatrix} \mathcal{I} & 0 \\ 0 & \mathcal{I} \end{bmatrix} \cdot \begin{bmatrix} \boldsymbol{J} \\ \boldsymbol{M} \end{bmatrix}(\boldsymbol{r}) = -\hat{\boldsymbol{n}} \times \begin{bmatrix} \boldsymbol{H}^{\mathrm{i}}(\boldsymbol{r}) \\ -\boldsymbol{E}^{\mathrm{i}}(\boldsymbol{r}) \end{bmatrix}, \tag{14}$$

where the same solution can be obtained trivially. We note that the "incident currents" $\{\hat{\boldsymbol{n}} \times \boldsymbol{H}^{\mathrm{i}}(\boldsymbol{r}), -\hat{\boldsymbol{n}} \times \boldsymbol{E}^{\mathrm{i}}(\boldsymbol{r})\}$ do not radiate and the conventional forms of the surface formulations satisfy the limit case mathematically. On the other hand, when they are discretized, these formulations fail to provide accurate results for the scattered fields from the low-contrast objects.

To understand the breakdown of the surface formulations, we note that any arbitrary solution can be decomposed as

$$\boldsymbol{J}(\boldsymbol{r}) = \hat{\boldsymbol{n}} \times \boldsymbol{H}(\boldsymbol{r}) = \hat{\boldsymbol{n}} \times \boldsymbol{H}^{\mathrm{i}}(\boldsymbol{r}) + \hat{\boldsymbol{n}} \times \boldsymbol{H}^{r}(\boldsymbol{r}), \tag{15}$$

$$\boldsymbol{M}(\boldsymbol{r}) = -\hat{\boldsymbol{n}} \times \boldsymbol{E}(\boldsymbol{r}) = -\hat{\boldsymbol{n}} \times \boldsymbol{E}^{\mathrm{i}}(\boldsymbol{r}) - \hat{\boldsymbol{n}} \times \boldsymbol{E}^{r}(\boldsymbol{r}), \tag{16}$$

where $\{\hat{\boldsymbol{n}} \times \boldsymbol{H}^{\mathrm{i}}(\boldsymbol{r}), \hat{\boldsymbol{n}} \times \boldsymbol{E}^{\mathrm{i}}(\boldsymbol{r})\}$ do not radiate. As the contrast goes to zero, these nonradiating currents dominate the total currents, while the radiating currents, i.e., $\{\hat{\boldsymbol{n}} \times \boldsymbol{H}^{r}(\boldsymbol{r}), \hat{\boldsymbol{n}} \times \boldsymbol{E}^{r}(\boldsymbol{r})\}$, tend to vanish. As an example, Fig. 1 presents the equivalent

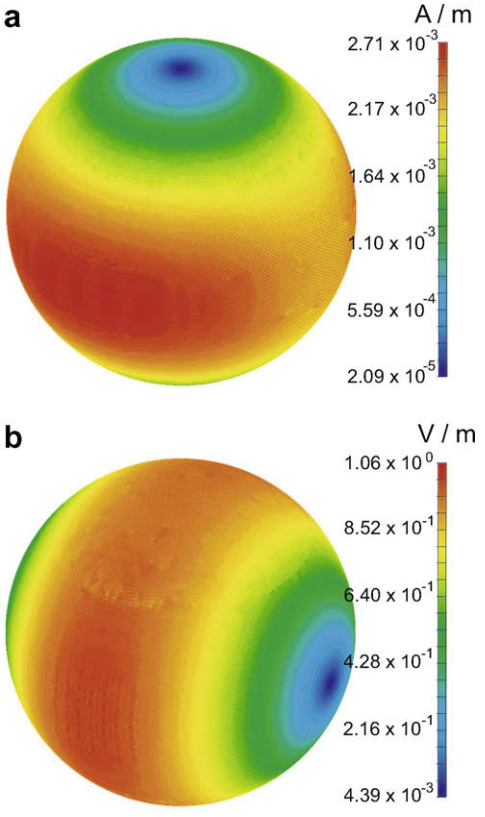

Fig. 1. Equivalent (a) electric and (b) magnetic currents on a sphere of radius 0.3 m illuminated by a plane wave at 6 GHz. The sphere is in free space and has a relative permittivity of $\epsilon_r = 1 + 10^{-4}$.

electric and magnetic currents on the surface of a dielectric sphere of radius 0.3 m illuminated by a plane wave at 6 GHz. The sphere is in free space and has a relative dielectric constant of $\epsilon_r = 1 + 10^{-4}$. The radiating parts of the currents are also depicted in Fig. 2. Comparing Figs. 1, and 2, we observe that the radiating currents form very small portions of the total currents. Therefore, when the total currents are solved by employing the conventional surface formulations, it becomes difficult to perform the calculations accurately enough to capture the small radiating currents properly. In other words, even though the surface currents $\boldsymbol{J}(\boldsymbol{r})$ and $\boldsymbol{M}(\boldsymbol{r})$ are computed with relatively small error, scattered fields may not be obtained accurately from them, since the radiating currents are numerically insignificant compared to the nonradiating currents [15].

3. Stabilization of surface formulations by extracting nonradiating currents

In order to calculate the scattered fields accurately, we extract the nonradiating parts of the currents and solve only the radiating currents as the unknowns of the problem. Stabilization of the T formulation in (9) leads to

$$\hat{\boldsymbol{t}} \cdot \begin{bmatrix} \eta_1\mathcal{T}_1 + \eta_2\mathcal{T}_2 & -(\mathcal{K}_1 + \mathcal{K}_2) \\ \eta_1\eta_2(\mathcal{K}_1 + \mathcal{K}_2) & \eta_2\mathcal{T}_1 + \eta_1\mathcal{T}_2 \end{bmatrix} \cdot \begin{bmatrix} \hat{\boldsymbol{n}} \times \boldsymbol{H}^r \\ -\hat{\boldsymbol{n}} \times \boldsymbol{E}^r \end{bmatrix} (\boldsymbol{r}) = \hat{\boldsymbol{t}} \cdot \begin{bmatrix} \eta_1\mathcal{T}_1 - \eta_2\mathcal{T}_2 & -(\mathcal{K}_1 - \mathcal{K}_2) \\ \eta_1\eta_2(\mathcal{K}_1 - \mathcal{K}_2) & \eta_2\mathcal{T}_1 - \eta_1\mathcal{T}_2 \end{bmatrix} \cdot \begin{bmatrix} \hat{\boldsymbol{n}} \times \boldsymbol{H}^{\mathrm{i}} \\ -\hat{\boldsymbol{n}} \times \boldsymbol{E}^{\mathrm{i}} \end{bmatrix} (\boldsymbol{r}), \tag{17}$$

which we call stable CTF (S-CTF). Similarly, stable CNF (S-CNF) is obtained from the N formulation in (11) as

$$\begin{aligned} -\begin{bmatrix} \mathcal{I} & 0 \\ 0 & \mathcal{I} \end{bmatrix} \cdot \begin{bmatrix} \hat{\boldsymbol{n}} \times \boldsymbol{H}^r \\ -\hat{\boldsymbol{n}} \times \boldsymbol{E}^r \end{bmatrix} (\boldsymbol{r}) + \hat{\boldsymbol{n}} \times \begin{bmatrix} \mathcal{K}_1 - \mathcal{K}_2 & \eta_1^{-1}\mathcal{T}_1 - \eta_2^{-1}\mathcal{T}_2 \\ -\eta_1\mathcal{T}_1 + \eta_2\mathcal{T}_2 & \mathcal{K}_1 - \mathcal{K}_2 \end{bmatrix} \cdot \begin{bmatrix} \hat{\boldsymbol{n}} \times \boldsymbol{H}^r \\ -\hat{\boldsymbol{n}} \times \boldsymbol{E}^r \end{bmatrix} (\boldsymbol{r}) \\ = -\hat{\boldsymbol{n}} \times \begin{bmatrix} \mathcal{K}_1 - \mathcal{K}_2 & \eta_1^{-1}\mathcal{T}_1 - \eta_2^{-1}\mathcal{T}_2 \\ -\eta_1\mathcal{T}_1 + \eta_2\mathcal{T}_2 & \mathcal{K}_1 - \mathcal{K}_2 \end{bmatrix} \cdot \begin{bmatrix} \hat{\boldsymbol{n}} \times \boldsymbol{H}^{\mathrm{i}} \\ -\hat{\boldsymbol{n}} \times \boldsymbol{E}^{\mathrm{i}} \end{bmatrix} (\boldsymbol{r}). \end{aligned} \tag{18}$$

We note that the LHSs of the stable formulations are the same as those of their conventional forms. In other words, the stabilization procedure only requires a modification on the RHSs of the formulations. On the RHSs, both S-CTF and S-CNF involve operators applied on the incident fields. Since these operators are already available, the stabilization does not require a significant cost in terms of the processing time and memory usage. The extra cost is only due to the calculation of the "modified" RHSs before the iterative solutions, which can be performed in negligible time compared to other parts of the implementations.

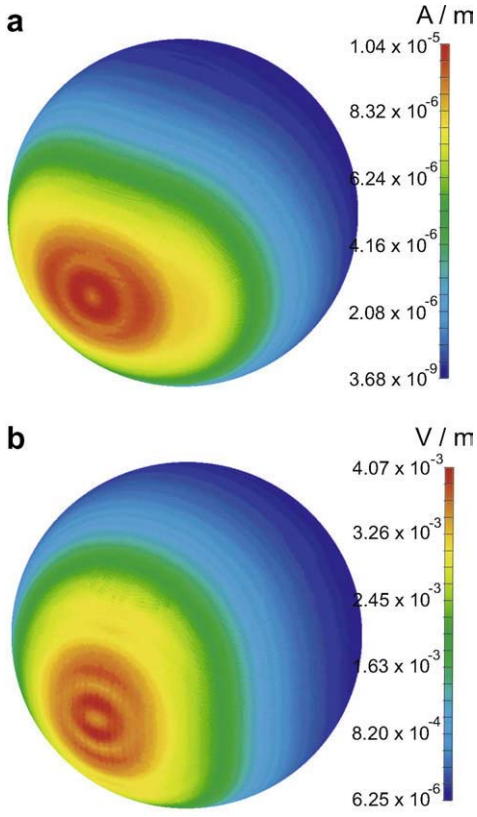

Fig. 2. Radiating parts of the (a) electric and (b) magnetic currents depicted in Fig. 1.

In their discrete forms, a direct approach to apply the operators on the incident fields is to expand the fields in a series of basis functions and perform MVMs. The expansion can be achieved by using the identity operators and solving the equation

$$\begin{bmatrix} \mathcal{I} & 0 \\ 0 & \mathcal{I} \end{bmatrix} \cdot \begin{bmatrix} \hat{\boldsymbol{n}} \times \boldsymbol{H}^{\mathrm{i}} \\ -\hat{\boldsymbol{n}} \times \boldsymbol{E}^{\mathrm{i}} \end{bmatrix} (\boldsymbol{r}) = \begin{bmatrix} \hat{\boldsymbol{n}} \times \boldsymbol{H}^{\mathrm{i}}(\boldsymbol{r}) \\ -\hat{\boldsymbol{n}} \times \boldsymbol{E}^{\mathrm{i}}(\boldsymbol{r}) \end{bmatrix} \tag{19}$$

with the method of moments. Using the RWG functions, the identity operators lead to sparse matrices and the discrete form of (19) can be written as

$$\begin{bmatrix} \bar{\boldsymbol{I}} & 0 \\ 0 & \bar{\boldsymbol{I}} \end{bmatrix} \cdot \begin{bmatrix} \boldsymbol{x}_i \\ \boldsymbol{y}_i \end{bmatrix} = \begin{bmatrix} \boldsymbol{v}_i \\ \boldsymbol{w}_i \end{bmatrix}, \tag{20}$$

where

$$\bar{\boldsymbol{I}}[m,n] = \langle \boldsymbol{t}_m(\boldsymbol{r}), \boldsymbol{b}_n(\boldsymbol{r}) \rangle, \tag{21}$$

$$\boldsymbol{v}_i[m] = \langle \boldsymbol{t}_m(\boldsymbol{r}), \hat{\boldsymbol{n}} \times \boldsymbol{H}^{\mathrm{i}}(\boldsymbol{r}) \rangle, \tag{22}$$

$$\boldsymbol{w}_i[m] = \langle \boldsymbol{t}_m(\boldsymbol{r}), -\hat{\boldsymbol{n}} \times \boldsymbol{E}^{\mathrm{i}}(\boldsymbol{r}) \rangle \tag{23}$$

and the vectors $\boldsymbol{x}_i$ and $\boldsymbol{y}_i$ represent the expansion coefficients, i.e.,

$$\hat{\boldsymbol{n}} \times \boldsymbol{H}^{\mathrm{i}}(\boldsymbol{r}) \approx \sum_{n=1}^{N} \boldsymbol{x}_i[n] \boldsymbol{b}_n(\boldsymbol{r}), \tag{24}$$

$$-\hat{\boldsymbol{n}} \times \boldsymbol{E}^{\mathrm{i}}(\boldsymbol{r}) \approx \sum_{n=1}^{N} \boldsymbol{y}_i[n] \boldsymbol{b}_n(\boldsymbol{r}). \tag{25}$$

In (21)–(25), $\boldsymbol{b}_n(\boldsymbol{r})$ and $\boldsymbol{t}_m(\boldsymbol{r})$ are the basis and testing functions, respectively, for $m, n = 1, 2, \ldots, N$. The solution of (19) usually requires negligible time; however, the use of the discretized identity operators may deteriorate the accuracy of the results. Although this is not critical for S-CNF, which already involves identity operators on the LHS, the accuracy of S-CTF can be affected significantly. Therefore, to further improve the accuracy of the T formulation, we can obtain the coefficients $\boldsymbol{x}_i$ and $\boldsymbol{y}_i$ by solving the discrete form of (13) [18]. This formulation, which is called the double-stabilized CTF (DS-CTF), is completely free of the identity operators at the cost of increased processing time due to the extra solution of the dense equation in (13).

The three stable formulations described above, namely, S-CNF, S-CTF, and DS-CTF, provide accurate results for moderately low-contrast problems that cannot be solved accurately with conventional formulations [18]. On the other hand, these stable formulations also have limitations; they break down when the contrast is decreased to very low values. In the next section, we introduce a novel stabilization procedure based on using fictitious incident fields to rearrange the RHSs of the formulations. This stabilization technique leads to more robust formulations that are valid for arbitrarily low contrasts.

4. A stabilization procedure based on fictitious incident fields

In both (17) and (18), the RHSs of the equations are obtained by applying the inner and outer operators on the incident fields. In addition, the operators are subtracted from each other so that the RHSs go to zero as the contrast decreases. Hence, we call these formulations operator-based stabilization formulations (OBSFs). Using OBSFs, the radiating parts of the currents can be computed accurately for low-contrast objects, i.e., when the radiating currents are numerically insignificant compared to the nonradiating currents. This is because the relatively large nonradiating currents are extracted, and only the radiating currents are solved for. Despite this corrective approach, even OBSFs break down and fail to provide accurate results for very low contrasts. The reason is the numerical errors arising during the computation of the RHSs of OBSFs, which become significant when the contrast decreases to very low values and renders the RHS vanishingly small.

To explain the numerical problems in OBSFs, we consider S-CTF in (17). The RHS of S-CTF is obtained by applying the integro-differential operators on the nonradiating currents, i.e., we compute

$$\mathrm{RHS}_{\text{S-CTF}} = \hat{\boldsymbol{t}} \cdot \begin{bmatrix} \eta_1 \mathcal{T}_1 & -\mathcal{K}_1 \\ \eta_1 \eta_2 \mathcal{K}_1 & \eta_2 \mathcal{T}_1 \end{bmatrix} \cdot \begin{bmatrix} \hat{\boldsymbol{n}} \times \boldsymbol{H}^{\mathrm{i}} \\ -\hat{\boldsymbol{n}} \times \boldsymbol{E}^{\mathrm{i}} \end{bmatrix} (\boldsymbol{r}) - \hat{\boldsymbol{t}} \cdot \begin{bmatrix} \eta_2 \mathcal{T}_2 & -\mathcal{K}_2 \\ \eta_1 \eta_2 \mathcal{K}_2 & \eta_1 \mathcal{T}_2 \end{bmatrix} \cdot \begin{bmatrix} \hat{\boldsymbol{n}} \times \boldsymbol{H}^{\mathrm{i}} \\ -\hat{\boldsymbol{n}} \times \boldsymbol{E}^{\mathrm{i}} \end{bmatrix} (\boldsymbol{r}). \tag{26}$$

Operators related to outer and inner media are applied on the tangential incident fields (nonradiating currents) in the first and the second terms of (26), respectively. Then, the second term is subtracted from the first term to compute the RHS. When the contrast is low, the RHS is small, but it is obtained by the subtraction of two terms that are relatively large. As detailed in Section 3, the discretized operators are applied on the incident fields by expanding the fields in a series of basis functions and performing MVMs. Therefore, the two terms of the RHS of S-CTF in (26) involve numerical errors. Depending on the discret-

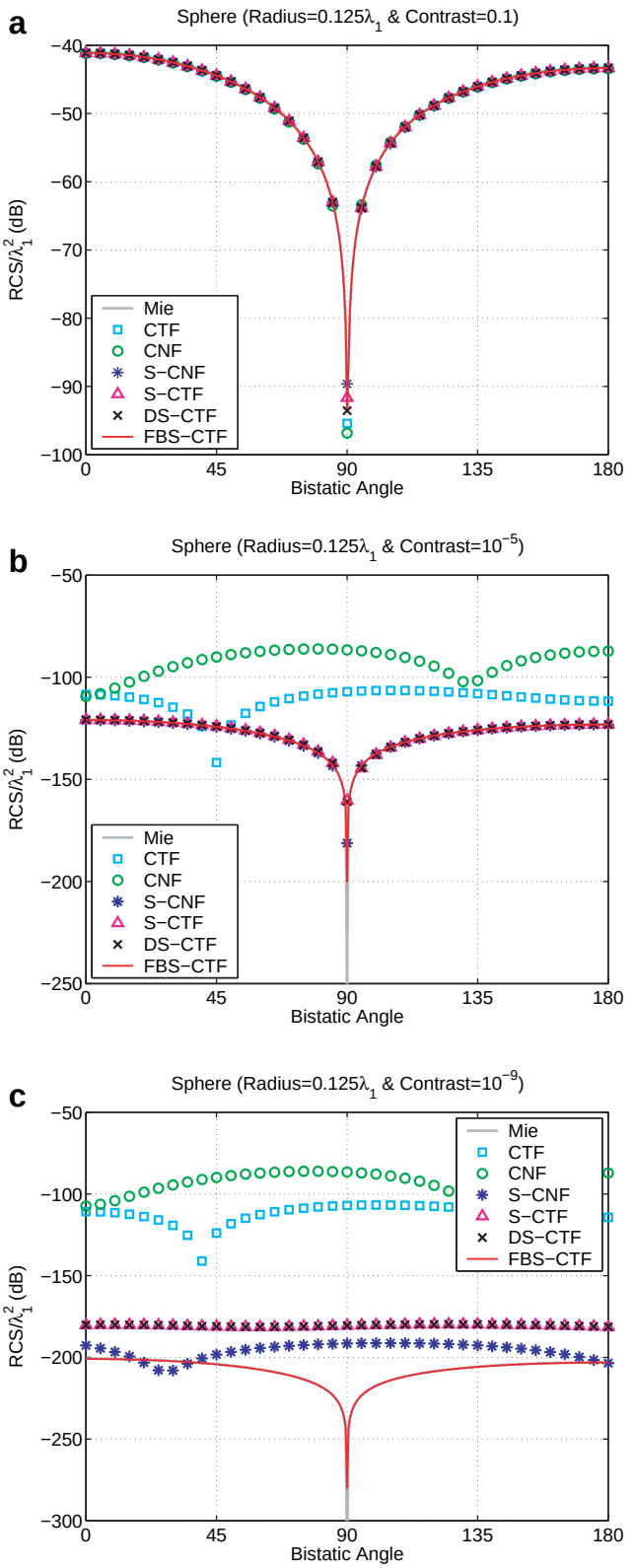

Fig. 3. Normalized bistatic RCS (RCS/λ_1^2 on the $\phi = 0^\circ$ plane) of a sphere of radius $0.125\lambda_1$, where λ_1 is the wavelength outside the sphere (free space), when the relative permittivity of the sphere is (a) $1 + 10^{-1}$, (b) $1 + 10^{-5}$, and (c) $1 + 10^{-9}$. The sphere is illuminated by a plane wave propagating in the z-direction with the electric field polarized in the x-direction.

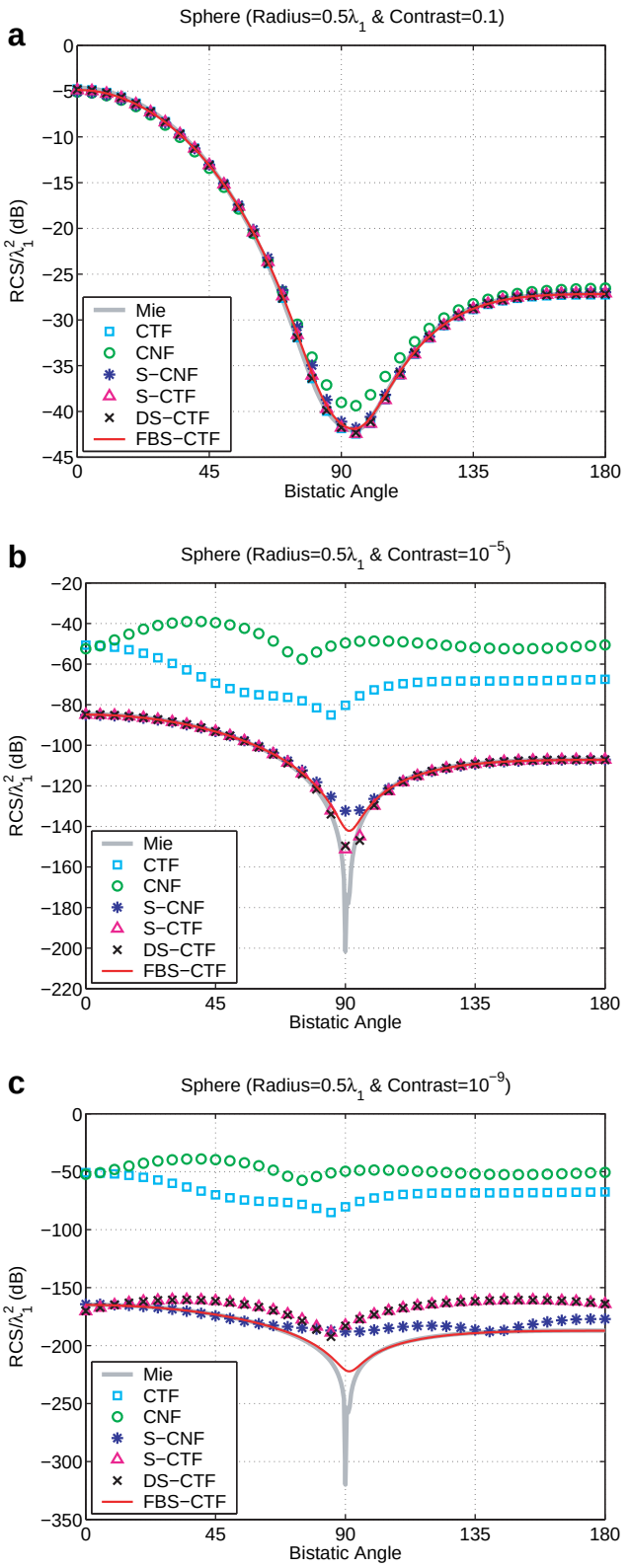

Fig. 4. Normalized bistatic RCS (RCS/λ_1^2 on the $\phi = 0^\circ$ plane) of a sphere of radius $0.5\lambda_1$, where λ_1 is the wavelength outside the sphere (free space), when the relative permittivity of the sphere is (a) $1 + 10^{-1}$, (b) $1 + 10^{-5}$, and (c) $1 + 10^{-9}$. The sphere is illuminated by a plane wave propagating in the z-direction with the electric field polarized in the x-direction.

ization and the accuracy of the MVMs, those errors can be significant and the RHS of S-CTF may not be calculated accurately when the contrast is very low, i.e., when the result of the subtraction is extremely small.

In general, OBSFs fail to provide accurate results when the contrast is decreased to very low values. Therefore, it is desirable to obtain a robust formulation that is valid for arbitrarily low contrasts. We achieve this by introducing fictitious fields and forming RHSs based on the difference of fields. This method leads to accurate calculation of the RHSs, even when the contrast is very low. We will present the stabilization procedure on the T formulation in (9), although it is also applicable to other T and N formulations.

When the incident fields are extracted from the LHS, the T formulation in (9) can be rewritten as

$$\hat{\boldsymbol{t}}\cdot\begin{bmatrix}\eta_1\mathcal{T}_1+\eta_2\mathcal{T}_2 & -(\mathcal{K}_1+\mathcal{K}_2)\\ \eta_1\eta_2(\mathcal{K}_1+\mathcal{K}_2) & \eta_2\mathcal{T}_1+\eta_1\mathcal{T}_2\end{bmatrix}\cdot\begin{bmatrix}\hat{\boldsymbol{n}}\times\boldsymbol{H}^r\\ -\hat{\boldsymbol{n}}\times\boldsymbol{E}^r\end{bmatrix}(\boldsymbol{r})=-0.5\hat{\boldsymbol{t}}\cdot\begin{bmatrix}\boldsymbol{E}^{\mathrm{i}}(\boldsymbol{r})\\ \eta_2\eta_1\boldsymbol{H}^{\mathrm{i}}(\boldsymbol{r})\end{bmatrix}-\hat{\boldsymbol{t}}\cdot\begin{bmatrix}\eta_2\mathcal{T}_2 & -\mathcal{K}_2\\ \eta_1\eta_2\mathcal{K}_2 & \eta_1\mathcal{T}_2\end{bmatrix}\cdot\begin{bmatrix}\hat{\boldsymbol{n}}\times\boldsymbol{H}^{\mathrm{i}}\\ -\hat{\boldsymbol{n}}\times\boldsymbol{E}^{\mathrm{i}}\end{bmatrix}(\boldsymbol{r}). \tag{27}$$

At this stage, we consider the incident fields as functions of medium parameters, i.e.,

$$\boldsymbol{E}^{\mathrm{i}}(\boldsymbol{r})=\boldsymbol{e}(\boldsymbol{r},\epsilon_1,\mu_1), \tag{28}$$

$$\boldsymbol{H}^{\mathrm{i}}(\boldsymbol{r})=\boldsymbol{h}(\boldsymbol{r},\epsilon_1,\mu_1). \tag{29}$$

Then, we define fictitious incident fields as

$$\boldsymbol{E}_2^{\mathrm{i}}(\boldsymbol{r})=\boldsymbol{e}(\boldsymbol{r},\epsilon_2,\mu_2), \tag{30}$$

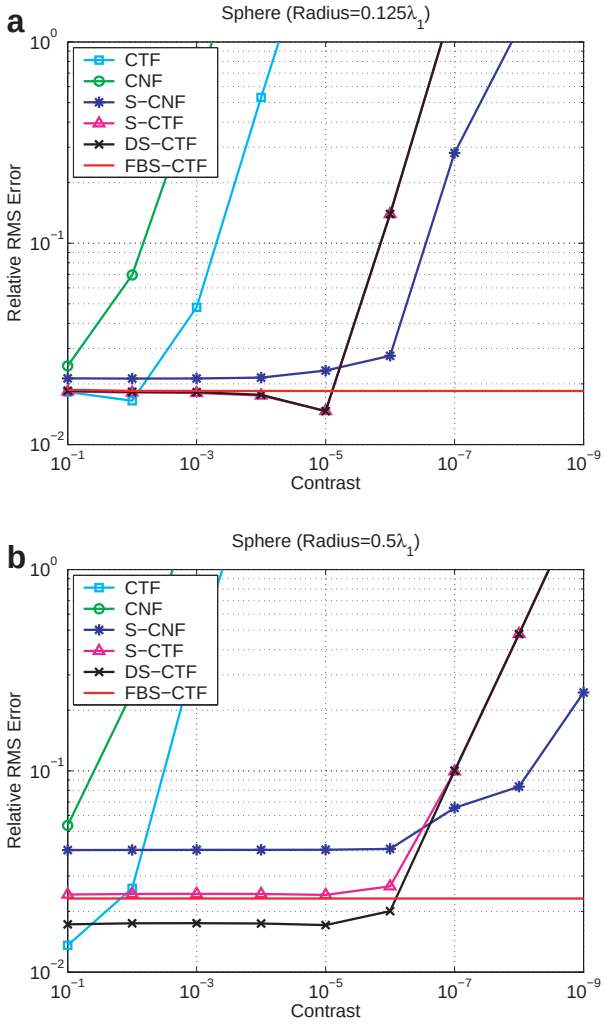

Fig. 5. Relative RMS error defined in (36) for the solutions of the scattering problems involving spheres of radii (a) $0.125\lambda_1$ and (b) $0.5\lambda_1$ with different contrasts, where λ_1 is the wavelength outside the sphere (free space).

$$\boldsymbol{H}_2^{\mathrm{i}}(\boldsymbol{r}) = \boldsymbol{h}(\boldsymbol{r}, \epsilon_2, \mu_2), \tag{31}$$

by using the parameters of the inner medium for the outside. This way, similar to the identities in (13), we have

$$\begin{Bmatrix} \hat{\boldsymbol{t}}\cdot \\ \hat{\boldsymbol{n}}\times \end{Bmatrix} \begin{bmatrix} \eta_2\mathcal{T}_2 & -\mathcal{K}_2 \\ \mathcal{K}_2 & \eta_2^{-1}\mathcal{T}_2 \end{bmatrix} \cdot \begin{bmatrix} \hat{\boldsymbol{n}}\times\boldsymbol{H}_2^{\mathrm{i}} \\ -\hat{\boldsymbol{n}}\times\boldsymbol{E}_2^{\mathrm{i}} \end{bmatrix}(\boldsymbol{r}) = -0.5 \begin{Bmatrix} \hat{\boldsymbol{t}}\cdot \\ \hat{\boldsymbol{n}}\times \end{Bmatrix} \begin{bmatrix} \boldsymbol{E}_2^{\mathrm{i}}(\boldsymbol{r}) \\ \boldsymbol{H}_2^{\mathrm{i}}(\boldsymbol{r}) \end{bmatrix}. \tag{32}$$

Finally, by adding and subtracting the terms of (32) in (27), we obtain

$$\hat{\boldsymbol{t}}\cdot \begin{bmatrix} \eta_1\mathcal{T}_1+\eta_2\mathcal{T}_2 & -(\mathcal{K}_1+\mathcal{K}_2) \\ \eta_1\eta_2(\mathcal{K}_1+\mathcal{K}_2) & \eta_2\mathcal{T}_1+\eta_1\mathcal{T}_2 \end{bmatrix} \cdot \begin{bmatrix} \hat{\boldsymbol{n}}\times\boldsymbol{H}^r \\ -\hat{\boldsymbol{n}}\times\boldsymbol{E}^r \end{bmatrix}(\boldsymbol{r}) = -0.5\hat{\boldsymbol{t}}\cdot \begin{bmatrix} \boldsymbol{E}^{\mathrm{i}}(\boldsymbol{r}) - \boldsymbol{E}_2^{\mathrm{i}}(\boldsymbol{r}) \\ \eta_2\eta_1(\boldsymbol{H}^{\mathrm{i}}(\boldsymbol{r}) - \boldsymbol{H}_2^{\mathrm{i}}(\boldsymbol{r})) \end{bmatrix} - \hat{\boldsymbol{t}}\cdot \begin{bmatrix} \eta_2\mathcal{T}_2 & -\mathcal{K}_2 \\ \eta_1\eta_2\mathcal{K}_2 & \eta_1\mathcal{T}_2 \end{bmatrix} \cdot \begin{bmatrix} \hat{\boldsymbol{n}}\times(\boldsymbol{H}^{\mathrm{i}} - \boldsymbol{H}_2^{\mathrm{i}}) \\ -\hat{\boldsymbol{n}}\times(\boldsymbol{E}^{\mathrm{i}} - \boldsymbol{E}_2^{\mathrm{i}}) \end{bmatrix}(\boldsymbol{r}), \tag{33}$$

which we call field-based-stabilized CTF (FBS-CTF). In contrast to OBSFs, FBS-CTF has a RHS obtained by subtracting the real and fictitious incident fields from each other. These subtractions can be performed analytically in the continuous space before the discretization. Then, the operators related to the inner medium are applied to compute the second term of the RHS in (33). We note that the RHS of FBS-CTF is obtained as the sum of two terms, i.e.,

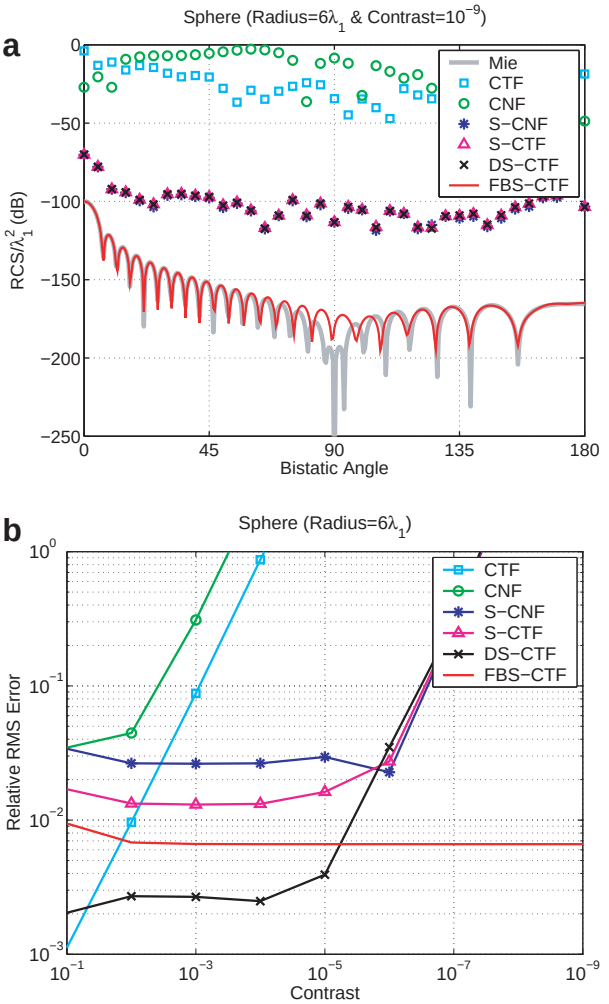

Fig. 6. (a) Normalized bistatic RCS (RCS/λ_1^2 on the $\phi = 0^\circ$ plane) of a sphere of radius $6\lambda_1$ and permittivity $1 + 10^{-9}$, where λ_1 is the wavelength outside the sphere (free space). The sphere is illuminated by a plane wave propagating in the z-direction with the electric field polarized in the x-direction. (b) Relative RMS error defined in (36) for the solution of a scattering problem involving a sphere of radius $6\lambda_1$ with different contrasts.

$$\mathrm{RHS}^{(1)}_{\text{FBS-CTF}} = -0.5\hat{\boldsymbol{t}} \cdot \begin{bmatrix} \boldsymbol{E}^{\mathrm{i}}(\boldsymbol{r}) - \boldsymbol{E}^{\mathrm{i}}_2(\boldsymbol{r}) \\ \eta_2\eta_1(\boldsymbol{H}^{\mathrm{i}}(\boldsymbol{r}) - \boldsymbol{H}^{\mathrm{i}}_2(\boldsymbol{r})) \end{bmatrix} \tag{34}$$

and

$$\mathrm{RHS}^{(2)}_{\text{FBS-CTF}} = -\hat{\boldsymbol{t}} \cdot \begin{bmatrix} \eta_2\mathcal{T}_2 & -\mathcal{K}_2 \\ \eta_1\eta_2\mathcal{K}_2 & \eta_1\mathcal{T}_2 \end{bmatrix} \cdot \begin{bmatrix} \hat{\boldsymbol{n}} \times (\boldsymbol{H}^{\mathrm{i}} - \boldsymbol{H}^{\mathrm{i}}_2) \\ -\hat{\boldsymbol{n}} \times (\boldsymbol{E}^{\mathrm{i}} - \boldsymbol{E}^{\mathrm{i}}_2) \end{bmatrix}(\boldsymbol{r}), \tag{35}$$

which are both small when the contrast is low. Consequently, the RHS can be calculated accurately for arbitrarily low contrasts, and it is sensitive to neither the discretization errors nor the numerical errors arising during MVMs. FBS-CTF can easily be obtained from the conventional CTF implementation and, similar to S-CTF and S-CNF, its extra cost is also negligible.

5. Results

To compare the accuracy of the formulations, we first present the results of the scattering problems involving a sphere of radius $0.125\lambda_1$ ("small sphere") and a sphere of radius $0.5\lambda_1$ ("medium sphere"), where λ_1 is the wavelength outside the spheres. The objects are in free space, they have various relative permittivities from $\epsilon_r = 1 + 10^{-1}$ to $\epsilon_r = 1 + 10^{-9}$, and they are illuminated by a plane wave propagating in the z direction with the electric field polarized in the x-direction. The same discretization (triangulation) is used for both spheres and the mesh size is about $\lambda_1/40$ for the small sphere and $\lambda_1/10$ for the medium sphere. For the small sphere, the dense $\lambda_1/40$ triangulation is required in order to model the sphere geometry accurately. We employ RWG basis functions and iteratively solve the matrix equations obtained by the discretization of various formulations. Both problems have the same matrix size of 1860×1860 and the matrix elements are computed directly with 10^{-2} relative error.

Fig. 3 depicts the bistatic radar cross section (RCS) of the small sphere for three different contrasts $(1 - \epsilon_r)$. Normalized RCS (RCS/λ_1^2) is plotted in decibels (dB) as a function of the observation angle on the $\phi = 0^\circ$ plane, where 0° corresponds to

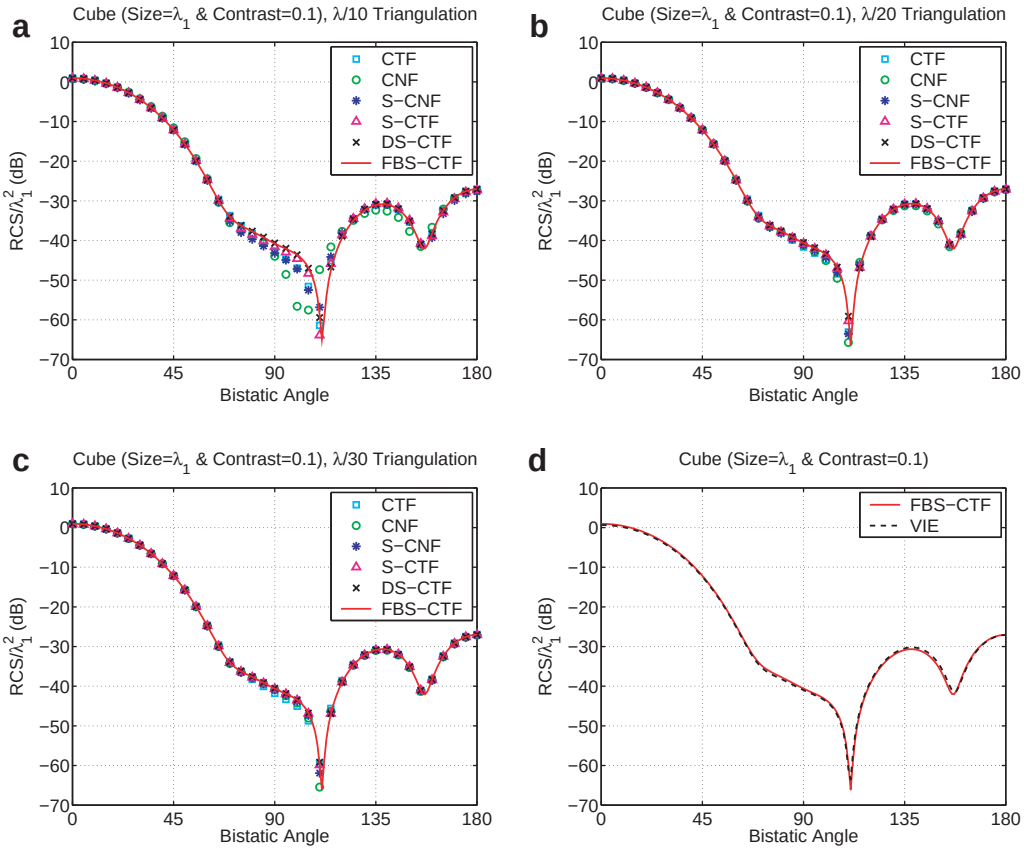

Fig. 7. Normalized bistatic RCS (RCS/λ_1^2 on the $\phi = 0^\circ$ plane) of a cube with edges of λ_1, where λ_1 is the wavelength outside the cube (free space). The relative permittivity of the cube is $1 + 10^{-1}$, and it is illuminated by a plane wave propagating in the z-direction with the electric field polarized in the x direction. RCS values are obtained by using surface formulations when the mesh size is (a) $\lambda_1/10$, (b) $\lambda_1/20$, and (c) $\lambda_1/30$. (d) RCS values obtained with FBS-CTF ($\lambda_1/30$ mesh size) and the electric-field VIE agree with each other.

the forward-scattering direction. For reference, the RCS values are also computed analytically by a Mie-series solution. When the contrast is 0.1, all of the formulations provide accurate results that are close to the analytical curve. As the contrast decreases to 10^{-5}, however, we observe that the conventional formulations, i.e., CTF and CNF, break down and cannot provide accurate results. When the contrast is further reduced to 10^{-9}, OBSFs also fail to agree with the analytical curve. For this extremely low contrast, the only formulation that provides accurate results is FBS-CTF.

Fig. 4 presents the bistatic RCS results for the medium sphere. Similar to the small sphere, conventional formulations and OBSFs encounter stability problems as the contrast is reduced down to 10^{-9}, while FBS-CTF is accurate for all contrasts. To further compare the formulations, Fig. 5 presents the relative root-mean-square (RMS) error as a function of the contrast. To calculate the error, we first compute the far-zone electric field on the $\phi = 0^\circ$ plane at $p = 360$ points from 0° to 180°. Then, the relative RMS error is defined as

$$e_{\mathrm{RMS}} = \frac{\|\boldsymbol{f}_{\mathrm{C}} - \boldsymbol{f}_{\mathrm{A}}\|_2}{\|\boldsymbol{f}_{\mathrm{A}}\|_2}, \tag{36}$$

where $\boldsymbol{f}_{\mathrm{C}}$ and $\boldsymbol{f}_{\mathrm{A}}$ are the computational and analytical values (complex arrays of p elements containing co-polar electric fields), respectively, and $\|\cdot\|_2$ represents the 2-norm of the arrays. Fig. 5(a) shows that the RMS errors of CTF and CNF increase sharply when the contrast decreases below 10^{-1}–10^{-2}, while OBSFs break down when the contrast is about 10^{-5}–10^{-6}. On the other hand, the error of FBS-CTF is almost constant with respect to the contrast. Similar observations can be made for the results of the medium sphere in Fig. 5(b).

Since the small sphere is discretized with very small triangles ($\lambda_1/40$) with respect to wavelength, the advantage of using DS-CTF or S-CTF compared to S-CNF is not obvious in Fig. 5(a). On the other hand, Fig. 5(b) shows that the three OBSFs show different characteristics for contrasts larger than the breakdown point. This is because the medium sphere is discretized with $\lambda_1/10$ mesh size and the effect of using the identity operators on the accuracy becomes visible. Using the identity operators on both RHS and LHS, S-CNF has larger error compared to S-CTF and DS-CTF. S-CTF has identity operators on the RHS and its accuracy is slightly worse than DS-CTF, which is completely free of the identity operators and the most accurate formulation

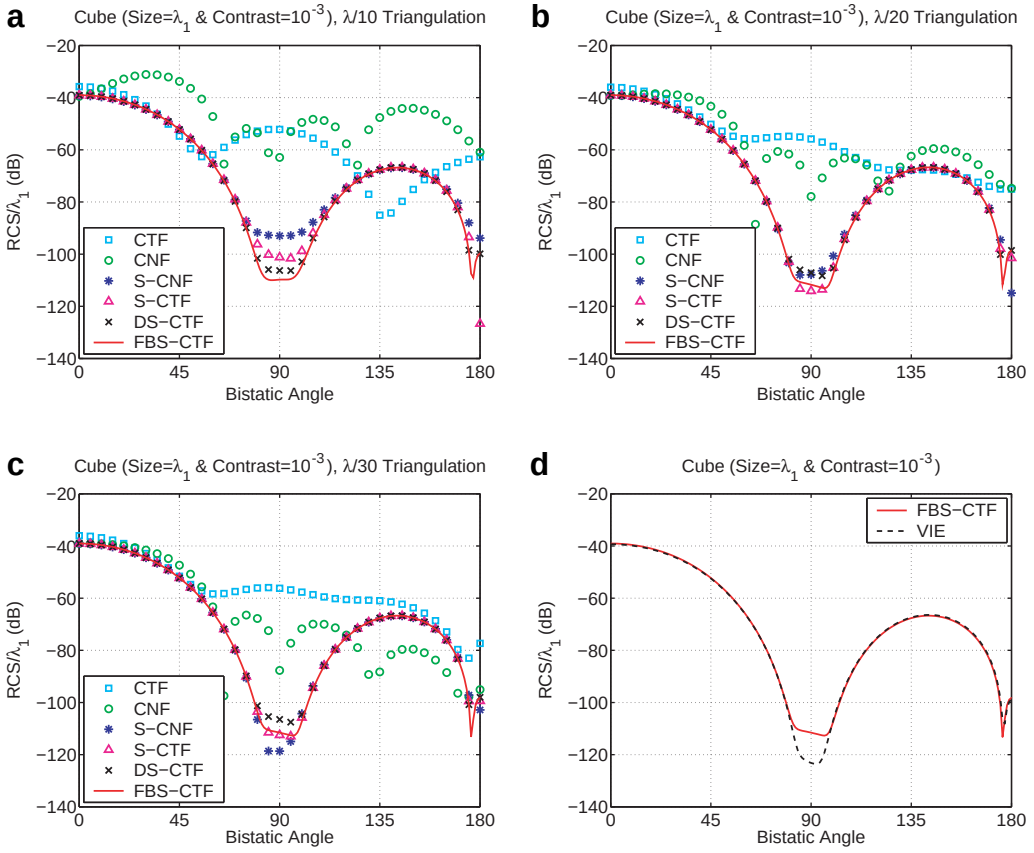

Fig. 8. Normalized bistatic RCS (RCS/λ_1^2 on the $\phi = 0^\circ$ plane) of a cube with edges of λ_1, where λ_1 is the wavelength outside the cube (free space). The relative permittivity of the cube is $1 + 10^{-3}$, and it is illuminated by a plane wave propagating in the z-direction with the electric field polarized in the x direction. RCS values are obtained by using surface formulations when the mesh size is (a) $\lambda_1/10$, (b) $\lambda_1/20$, and (c) $\lambda_1/30$. (d) RCS values obtained with FBS-CTF ($\lambda_1/30$ mesh size) and the electric-field VIE agree with each other.

up to breakdown point. We note that DS-CTF requires twice the processing time of S-CTF. In addition, S-CNF leads to better-conditioned matrix equations that are easier and more efficient to solve iteratively. Therefore, there exists a tradeoff between the accuracy and efficiency of the solutions. Finally, in Fig. 5(b), we note that DS-CTF is even better than FBS-CTF for contrasts 10^{-1}–10^{-6}, since FBS-CTF also uses identity operators on the LHS to apply the operators on the difference of real and fictitious incident fields.

For larger problems, we implement MLFMA to accelerate the iterative solutions of the dielectric formulations. Efficient and accurate diagonalization of the operators can be found in various references [3,28]. As an example, we present the results of a sphere of radius $6\lambda_1$ discretized with 264,006 RWG functions. Scattering problems are solved by 5-level MLFMA, where the near-field interactions are calculated with 1% error and the far-field interactions are computed with three digits of accuracy. Fig. 6(a) depicts the bistatic RCS values on the $\phi = 0^\circ$ plane when the sphere is illuminated by a plane wave propagating in the z-direction with the electric field polarized in the x-direction and the contrast of the sphere is 10^{-9}. We observe that all formulations except for the FBS-CTF fail to provide accurate results compared to Mie-series solution. As presented in Fig. 6(b), the accuracy of FBS-CTF is stable for all values of the contrast from 10^{-1} to 10^{-9}. OBSFs are also stable in the 10^{-1}–10^{-5} range, while they offer different levels of accuracy depending on the use of the identity operators. However, they break down when the contrast decreases below 10^{-5}. Finally, as in the previous examples, the conventional CTF and CNF break down immediately below 10^{-1} contrast, testifying to the need for stabilized formulations.

FBS-CTF provides accurate solutions of low-contrast problems with negligible extra computational cost. As an example, we consider the solution of a scattering problem involving a sphere of radius $6\lambda_1$ and contrast 10^{-3}. The problem is discretized with 264,006 unknowns and solved by 5-level MLFMA on a 2.0 GHz AMD Opteron 870 processor. To obtain the RHS of FBS-CTF, the difference of incident and fictitious fields in (35) is expanded in a series of basis functions by solving a sparse matrix equation involving identity terms similar to (20). Using the conjugate-gradient-squared (CGS) method, the number of iterations to reduce the residual error to less than 10^{-6} is 8, and the solution of the sparse matrix equation is achieved in only 1 s. Then, the inner operators are applied on the result of the subtraction via a MVM in 137 s. As a result, the processing time to compute the RHS of FBS-CTF, which is the extra cost of the stabilization procedure, is only 138 s. Solution of FBS-CTF is also performed by using the CGS method, where each iteration involves two MVMs, and each MVM requires $2 \times 137 = 274$

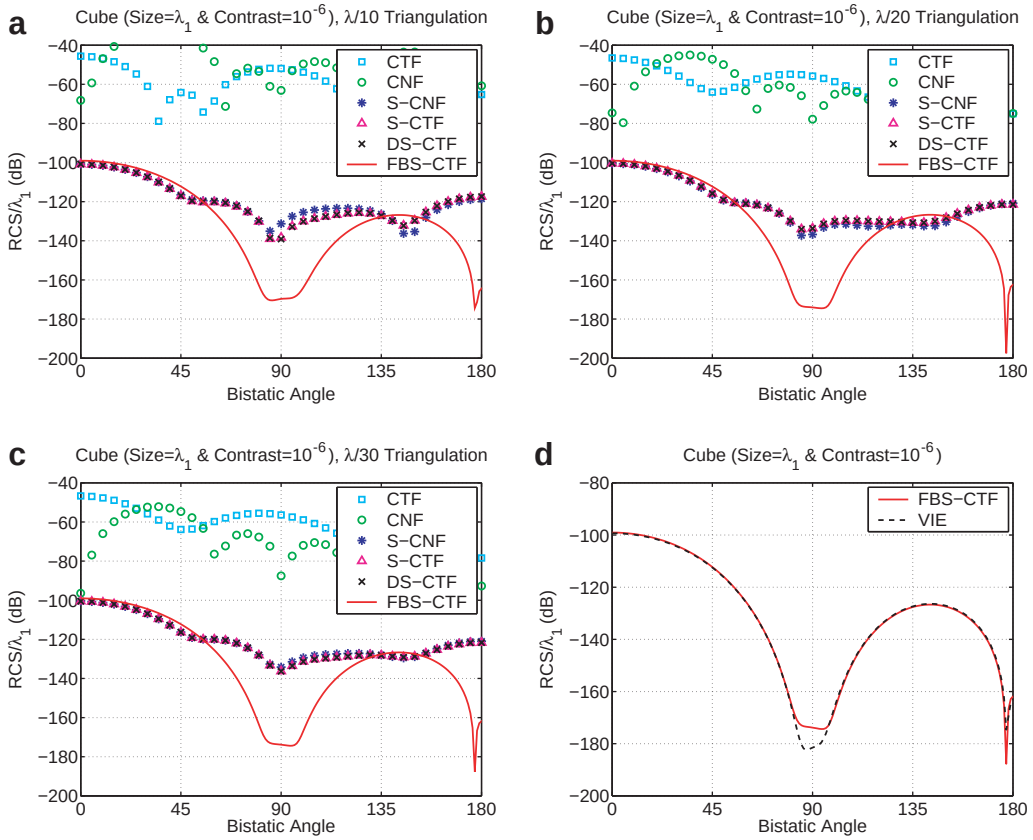

Fig. 9. Normalized bistatic RCS (RCS/λ_1^2 on the $\phi = 0^\circ$ plane) of a cube with edges of λ_1, where λ_1 is the wavelength outside the cube (free space). The relative permittivity of the cube is $1 + 10^{-6}$, and it is illuminated by a plane wave propagating in the z direction with the electric field polarized in the x-direction. RCS values are obtained by using surface formulations when the mesh size is (a) $\lambda_1/10$, (b) $\lambda_1/20$, and (c) $\lambda_1/30$. (d) RCS values obtained with FBS-CTF ($\lambda_1/30$ mesh size) and the electric-field VIE agree with each other.

seconds, since both inner and outer operators are applied. Then, each CGS iteration is performed in 548 s. Besides, the number of iterations to reduce the residual error to less than 10^{-3} is 270, and the solution time of FBS-CTF is about 41 h. The solution time can be reduced by accelerating the iterative convergence via preconditioners or by parallelizing the MLFMA implementation on a cluster of processors. Nevertheless, the stabilization procedure, which requires only 138 s, is always negligible compared to the solution part. Finally, the stabilization procedure does not change the number of iterations significantly since only the RHS is modified. For the solution of the same problem, the conventional CTF requires 285 CGS iterations.

In addition to the spheres with smooth surfaces, we present the results of the scattering problems involving a cube with edges of λ_1, where λ_1 is the wavelength outside the object. The cube is in free space and it is illuminated by a plane wave propagating in the z-direction with the electric field polarized in the x-direction. We consider three different relative permittivities for the cube, i.e., $\epsilon_r = 1 + 10^{-1}$, $\epsilon_r = 1 + 10^{-3}$, and $\epsilon_r = 1 + 10^{-6}$, corresponding to 10^{-1}, 10^{-3}, and 10^{-6} contrasts, respectively. In addition, each problem is discretized with three different triangulations with mesh sizes $\lambda_1/10$, $\lambda_1/20$, and $\lambda_1/30$. Scattering problems are solved by FMM, where the near-field interactions are calculated with 1% error and the far-field interactions are computed with three digits of accuracy.

Fig. 7 presents the normalized RCS (RCS/λ_1^2) in dB as a function of the observation angle on the $\phi = 0^\circ$ plane, where 0° corresponds to the forward-scattering direction. The contrast of the cube is 10^{-1}. As depicted in Fig. 7(a), there are relatively small discrepancies among the results obtained by using different formulations with $\lambda_1/10$ mesh size. On the other hand, when the discretization quality is improved by decreasing the mesh size to $\lambda_1/20$ and $\lambda_1/30$, all solutions converge to each other as depicted in Fig. 7(b) and Fig. 7(c), respectively. Finally, in Fig. 7(d), we compare the RCS values obtained by using FBS-CTF and $\lambda_1/30$ mesh size with those obtained by using the electric-field VIE [29], which is immune to low-contrast problems. Fig. 7(d) confirms that FBS-CTF and the other surface formulations are accurate when the contrast of the cube is 10^{-1}.

Fig. 8 compares the bistatic RCS values obtained by various formulations as the contrast of the cube is decreased to 10^{-3}. In this case, RCS values obtained by using the conventional formulations, namely, CTF and CNF, are inconsistent with the values obtained by using the stable formulations, i.e., S-CNF, S-CTF, DS-CTF and FBS-CTF. In addition, RCS results obtained with the conventional and stable formulations do not converge to each other, even when the mesh size is decreased to $\lambda_1/30$. As demonstrated in Fig. 8(d), FBS-CTF (and other stable formulations) are consistent with VIE. Hence, we conclude that the stable formulations are accurate, while CTF and CNF break down when the contrast of the cube is 10^{-3}. Finally, Fig. 9 presents the bistatic RCS results, when the contrast of the cube is very low, i.e., 10^{-6}. As opposed to the previous examples, RCS values obtained with OBSFs (S-CNF, S-CTF, and DS-CTF) and FBS-CTF do not converge to each other, even when the mesh size is $\lambda_1/30$. In Fig. 9(d), we again compare FBS-CTF with VIE, where the two formulations agree well with each other. This proves that only FBS-CTF provides accurate results, while the other surface formulations break down when the contrast is 10^{-6}.

6. Conclusion

In this paper, a novel stabilization technique is introduced for the accurate surface formulations of dielectric bodies with arbitrarily low contrasts. Similar to previous stabilization procedures, the technique is based on extracting the nonradiating currents and solving the modified equations to obtain the radiating currents. In addition, this technique involves the use of fictitious incident fields to rearrange the RHSs of the equations appropriately. We apply the stabilization to a combined T formulation although it is also applicable to other T the N formulations. The stabilization is easy to implement by modifying the existing codes for conventional formulations. In addition, the extra cost due to the stabilization is negligible. Our results show that the stabilized equation, namely, FBS-CTF, provides accurate results even for extremely low-contrast objects, such as a sphere with a contrast of 10^{-9}.

Acknowledgments

This work was supported by the Scientific and Technical Research Council of Turkey (TUBITAK) under Research Grant 105E172, by the Turkish Academy of Sciences in the framework of the Young Scientist Award Program (LG/TUBA-GEBIP/2002-1-12), and by contracts from ASELSAN and SSM.

References

[1] A.J. Poggio, E.K. Miller, Integral equation solutions of three-dimensional scattering problems, in: R. Mittra (Ed.), Computer Techniques for Electromagnetics, Pergamon Press, Oxford, 1973 (Chapter 4).
[2] S.M. Rao, D.R. Wilton, E-field, H-field, and combined field solution for arbitrarily shaped three-dimensional dielectric bodies, Electromagnetics 10 (4) (1990) 407–421.
[3] X.-Q. Sheng, J.-M. Jin, J. Song, W.C. Chew, C.-C. Lu, Solution of combined-field integral equation using multilevel fast multipole algorithm for scattering by homogeneous bodies, IEEE Trans. Antennas Propagat. 46 (11) (1998) 1718–1726.
[4] P. Ylä-Oijala, M. Taskinen, Application of combined field integral equation for electromagnetic scattering by dielectric and composite objects, IEEE Trans. Antennas Propagat. 53 (3) (2005) 1168–1173.
[5] P. Ylä-Oijala, M. Taskinen, Well-conditioned Müller formulation for electromagnetic scattering by dielectric objects, IEEE Trans. Antennas Propagat. 53 (10) (2005) 3316–3323.
[6] P. Ylä-Oijala, M. Taskinen, S. Järvenpää, Surface integral equation formulations for solving electromagnetic scattering problems with iterative methods, Radio Sci. 40 (RS6002) (2005), doi:10.1029/2004RS003169.

[7] T.W. Lloyd, J.M. Song, M. Yang, Numerical study of surface integral formulations for low-contrast objects, IEEE Antennas Wireless Propagat. Lett. 4 (2005) 482–485.
[8] P. Ylä-Oijala, M. Taskinen, Improving conditioning of electromagnetic surface integral equations using normalized field quantities, IEEE Trans. Antennas Propagat. 55 (1) (2007) 178–185.
[9] P. Loschialpo, D.W. Forester, J. Schelleng, Anomalous transmission through near unit index contrast dielectric photonic crystals, J. Appl. Phys. 86 (10) (1999) 5342–5347.
[10] E.S. Thiele, Scattering of Electromagnetic Radiation by Complex Microstructures in the Resonant Regime, Ph.D. Thesis, University of Pennsylvania, 1998.
[11] D.A. Hill, Electromagnetic scattering by buried objects of low contrast, IEEE Trans. Geosci. Remote Sens. 26 (2) (1988) 195–203.
[12] S.H. Tseng, A. Taflove, D. Maitland, V. Backman, Pseudospectral time domain simulations of multiple light scattering in three-dimensional macroscopic random media, Radio Sci. 41 (RS4009) (2006), doi:10.1029/2005RS003408.
[13] M. Hammer, D. Schweitzer, B. Michel, E. Thamm, A. Kolb, Single scattering by red blood cells, Appl. Optics 37 (31) (1998) 7410–7418.
[14] J.Q. Lu, P. Yang, X.-H. Hu, Simulations of light scattering from a biconcave red blood cell using the finite-difference time-domain method, J. Biomed. Opt. 10 (2) (2005) 024022.
[15] P.M. Goggans, A. Glisson, A surface integral equation formulation for low contrast scatterers based on radiation currents, ACES J. 10 (1995) 15–18.
[16] Ö. Ergül, L. Gürel, Improving the accuracy of the surface integral equations for low-contrast dielectric scatterers. in: Proc. IEEE Antennas and Propagation Soc. Int. Symp., 2007, pp. 4853–4856
[17] Ö. Ergül, L. Gürel, Accurate solutions of scattering problems involving low-contrast dielectric objects with surface integral equations, in: Second European Conference on Antennas and Propagation (EuCAP), Edinburgh, UK, November 2007.
[18] Ö. Ergül, L. Gürel, Stabilization of integral-equation formulations for accurate solution of scattering problems involving low-contrast dielectric objects, IEEE Trans. Antennas Propagat. 56 (3) (2008) 799–805.
[19] L. Gürel, Ö. Ergül, Comparisons of FMM implementations employing different formulations and iterative solvers, in: Proc. IEEE Antennas and Propagation Soc. Int. Symp., vol. 1, 2003, pp. 19–22.
[20] Ö. Ergül, L. Gürel, Investigation of the inaccuracy of the MFIE discretized with the RWG basis functions, in: Proc. IEEE Antennas and Propagation Soc. Int. Symp., vol. 3, 2004, pp. 3393–3396.
[21] Ö. Ergül, L. Gürel, Improving the accuracy of the MFIE with the choice of basis functions, in: Proc. IEEE Antennas and Propagation Soc. Int. Symp., vol. 3, 2004, pp. 3389–3392.
[22] S.M. Rao, D.R. Wilton, A.W. Glisson, Electromagnetic scattering by surfaces of arbitrary shape, IEEE Trans. Antennas Propagat. AP-30 (3) (1982) 409–418.
[23] Ö. Ergül, L. Gürel, The use of curl-conforming basis functions for the magnetic-field integral equation, IEEE Trans. Antennas Propagat. 54 (7) (2006) 1917–1926.
[24] E. Úbeda, J.M. Rius, Novel monopolar MFIE MoM-discretization for the scattering analysis of small objects, IEEE Trans. Antennas Propagat. 54 (1) (2006) 50–57.
[25] Ö. Ergül, L. Gürel, Improving the accuracy of the magnetic field integral equation with the linear–linear basis functions, Radio Sci. 41 (RS4004) (2006), doi:10.1029/2005RS003307.
[26] Ö. Ergül, L. Gürel, Linear–linear basis functions for MLFMA solutions of magnetic-field and combined-field integral equations, IEEE Trans. Antennas Propagat. 55 (4) (2007) 1103–1110.
[27] C.P. Davis, K.F. Warnick, High-order convergence with a low-order discretization of the 2-D MFIE, IEEE Antennas Wireless Propagat. Lett. 3 (2004) 355–358.
[28] Ö. Ergül, L. Gürel, Fast and accurate solutions of scattering problems involving dielectric objects with moderate and low contrasts, in: Proc. 2007 Computational Electromagnetics Workshop, 2007, pp. 59–64.
[29] D.H. Schaubert, D.R. Wilton, A.W. Glisson, A tedrahedral modeling method for electromagnetic scattering by arbitrarily shaped inhomogeneous dielectric bodies, IEEE Trans. Antennas Propagat. AP-32 (1) (1984) 77–85.